Supporting Information

Enami et al. 10.1073/pnas.1314885111

SI Text

Mass spectrometers detect net charge. Therefore, the first step is separation of preexisting anions from cations in the inflowing solutions (1, 2). This is accomplished via the pneumatic breakup of the aqueous jet by a fast nebulizer gas that shears the outermost layers into submicron droplets carrying net charges of either sign.

i) We have demonstrated experimentally that the charges we detect are largely produced pneumatically by showing that ion signals (*i*) increase at higher gas velocities v and (*ii*) extrapolate to zero as $v \rightarrow 0$ (2).

ii) We have confirmed that the modest polarizations of the microjets do not affect the observed chemistries (3–7) by showing that the kinetics of the reaction of dissolved α-tocopherol with gaseous ozone, determined on the basis of negative and positive ion detection, were identical (6).

iii) Because the nebulizer gas can fragment the first-generation microdroplets but not the smaller charged droplets for hydrodynamic reasons (8, 9), the creation of net charge is a one-time event.

iv) Second-generation droplets may lose mass via solvent evaporation in the dry $N_2(g)$ atmosphere but retain their excess charges. We have verified that the net charge carried by the ensemble of microdroplets is proportional to the concentrations of the reactant, intermediates, and products formed on the surface of the jet during reactive gas–liquid collisions.

v) The concentration dependences observed in present experiments strongly support our assumption that the detected species are produced on the surface of the intact jet (whose composition is identical to that of the injected solution) rather than on the ensemble of daughter droplets (whose compositions span the broad distributions generated by random solvent evaporation) (3–5, 10). This finding corroborates previous reports showing that the titration curves of carboxylic acids and trimethylamine obtained from the dependence of the carboxylate and trimethylammonium mass spectrometric signals as functions of pH in this setup are identical to those determined by standard titrations in the injected solutions, both leading to the ionization constants reported in the literature, i.e., $pK_a = 4.8$ and 9.8, respectively (3, 4).

vi) A key feature of our instrument is that the jet issuing from the nozzle source is orthogonal to the polarized inlet to the mass spectrometer (Figs. S1 and S2). Therefore, the charged droplets deflected toward the mass spectrometer preferentially originate from the interfacial layers of the jet, whereas its core maintains its forward trajectory. The ejection of dissolved ions to the gas phase takes place from the smallest droplets at the end of a sequence of events comprising extensive solvent evaporation and net charge crowding in shrinking droplets that become unstable and undergo a cascade of Coulomb explosions (11, 12). Finally, gas-phase ions are sorted out and detected by the online mass spectrometer.

vii) The possibility that the species we monitor were produced in the reactions of gases with the highly concentrated, high surface-to-volume small droplets undergoing Coulomb explosions is excluded by experimental evidence. We found that product signal intensities decrease by injecting the reactive gases 5 mm and 10 mm downstream (relative to the standard position of the gas injector) along the jet direction (13). This is the expected outcome of a process in which products are formed in collisions of the reactive gases with the intact jet. The fact that product formation is not suppressed completely by shifting the gas injector downstream is ascribed to the gas beams losing their collimation by turbulent mixing with the nebulizer gas at the reaction zone.

viii) Previous data analysis based on mass balances and the kinetic theory of gases (14) suggest that the thickness of the interfacial layers sampled in these experiments is less than 1 nm (4, 15). More compellingly, we recently showed that the depth of the interfacial layers sampled in our experiments is controllable as a function of nebulizer gas velocity v (2). Under the present high v (~160 m/s) condition, ions residing at the topmost layers of the air−water interface are preferentially detected as mass signals (2).

All the experiments were performed at Kyoto University. Conditions in the present experiments were as follows: drying gas flow rate, 13 $L \cdot min^{-1}$; drying gas temperature, 340 °C; inlet voltage, + 3.5 kV relative to ground; fragmentor voltage value, 80 V. $Fe(II)Cl_2 \cdot 4H_2O$ (>99%; Sigma–Aldrich), hydrogen peroxide [extra pure reagent, 30% (wt) solution; Nacalai Tesque], *tert*-butanol (>99%; Tokyo Chemical Industry), DMSO (>99.9%; Sigma–Aldrich), NaCl (>99%; Sigma–Aldrich), HCl [35% (wt) solution; Nacalai Tesque], and NaOH (10 N solution; Nacalai Tesque) were used as received. All solutions were prepared in purified water (resistivity ≥18.2 MΩ cm at 298 K) from a Millipore Milli-Q water purification system. All experiments were performed at 293 ± 2 K.

1. Enami S, Colussi AJ (2013) Long-range Hofmeister effects of anionic and cationic amphiphiles. *J Phys Chem B* 117(20):6276–6281.
2. Enami S, Colussi AJ (2013) Long-range specific ion-ion interactions in hydrogen-bonded liquid films. *J Chem Phys* 138(18):184706.
3. Mishra H, et al. (2012) Brønsted basicity of the air-water interface. *Proc Natl Acad Sci USA* 109(46):18679–18683.
4. Enami S, Hoffmann MR, Colussi AJ (2010) Proton availability at the air/water interface. *J Phys Chem Lett* 1(10):1599–1604.
5. Enami S, Hoffmann MR, Colussi AJ (2008) Acidity enhances the formation of a persistent ozonide at aqueous ascorbate/ozone gas interfaces. *Proc Natl Acad Sci USA* 105(21):7365–7369.
6. Enami S, Hoffmann MR, Colussi AJ (2009) How phenol and alpha-tocopherol react with ambient ozone at gas/liquid interfaces. *J Phys Chem A* 113(25):7002–7010.
7. Enami S, Vecitis CD, Cheng J, Hoffmann MR, Colussi AJ (2007) Electrospray mass spectrometric detection of products and short-lived intermediates in aqueous aerosol microdroplets exposed to a reactive gas. *J Phys Chem A* 111(50):13032–13037.
8. Lasheras JC, Villermaux E, Hopfinger EJ (1998) Break-up and atomization of a round water jet by a high-speed annular air jet. *J Fluid Mech* 357:351–379.
9. Gorokhovski MA, Saveliev VL (2003) Analyses of Kolmogorov's model of breakup and its application into Lagrangian computation of liquid sprays under air-blast atomization. *Phys Fluids* 15(1):184–192.
10. Mishra H, et al. (2012) Anions dramatically enhance proton transfer through aqueous interfaces. *Proc Natl Acad Sci USA* 109(26):10228–10232.
11. Iribarne JV, Thomson BA (1976) On the evaporation of small ions from charged droplets. *J Chem Phys* 64:2287.
12. Kebarle P, Peschke M (2000) On the mechanisms by which the charged droplets produced by electrospray lead to gas phase ions. *Anal Chim Acta* 406(1):11–35.
13. Enami S, Vecitis CD, Cheng J, Hoffmann MR, Colussi AJ (2007) Global inorganic source of atmospheric bromine. *J Phys Chem A* 111(36):8749–8752.
14. Davidovits P, Kolb CE, Williams LR, Jayne JT, Worsnop DR (2006) Mass accommodation and chemical reactions at gas-liquid interfaces. *Chem Rev* 106(4):1323–1354.
15. Enami S, Stewart LA, Hoffmann MR, Colussi AJ (2010) Superacid chemistry on mildly acidic water. *J Phys Chem Lett* 1(24):3488–3493.

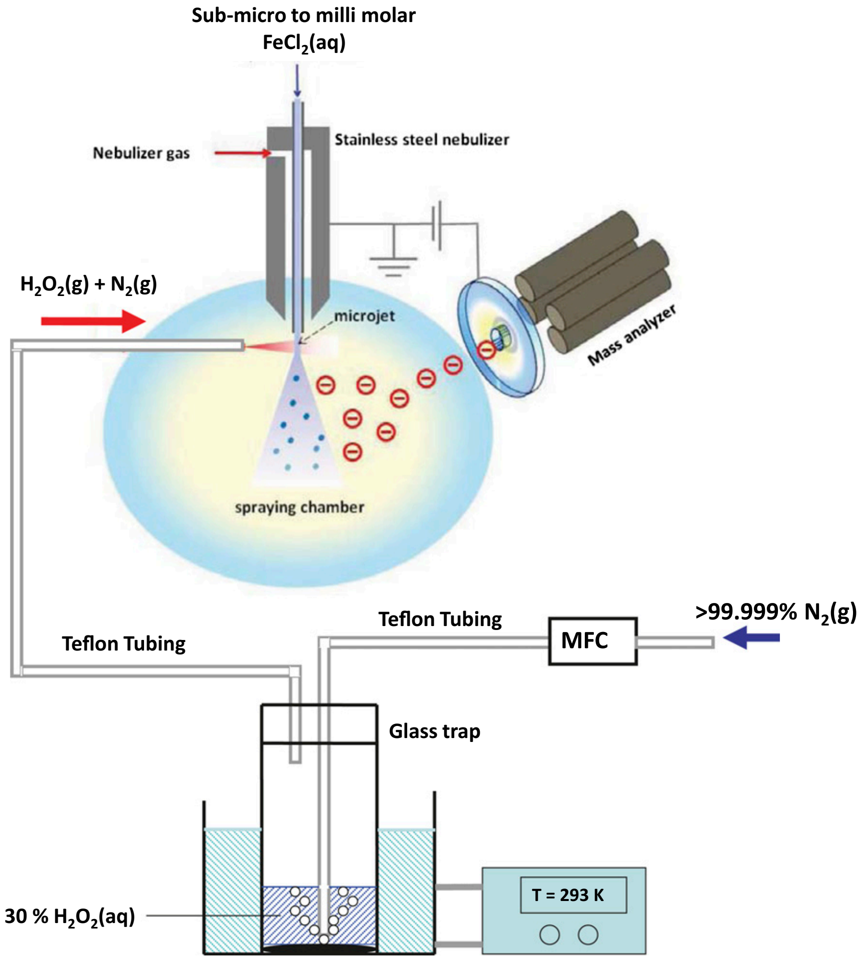

Fig. S1. Schematic diagram of the experimental setup for the $H_2O_2(g)$ + $FeCl_2(aq)$ microjet system. MFC, mass flow controller.

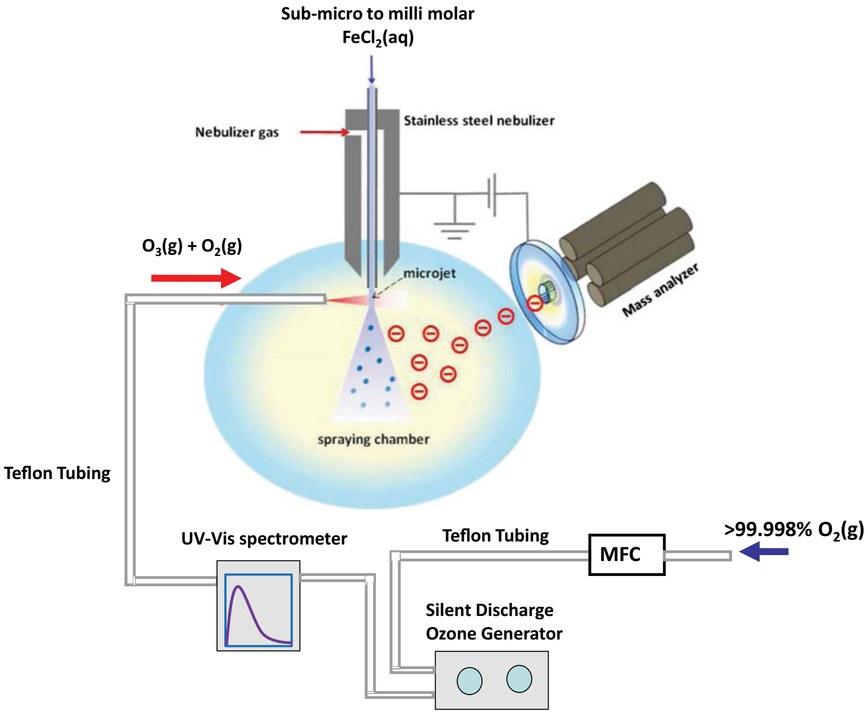

Fig. S2. Schematic diagram of the experimental setup for the $O_3(g) + FeCl_2(aq)$ microjet system. MFC, mass flow controller.

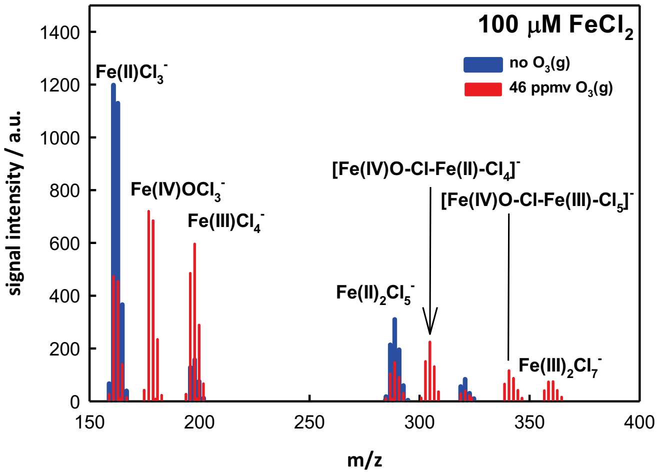

Fig. S3. Negative ion electrospray mass spectra of aqueous microjets containing 100 μM $FeCl_2$ in the absence/presence of $O_3(g)$ for ∼10–50 μs.

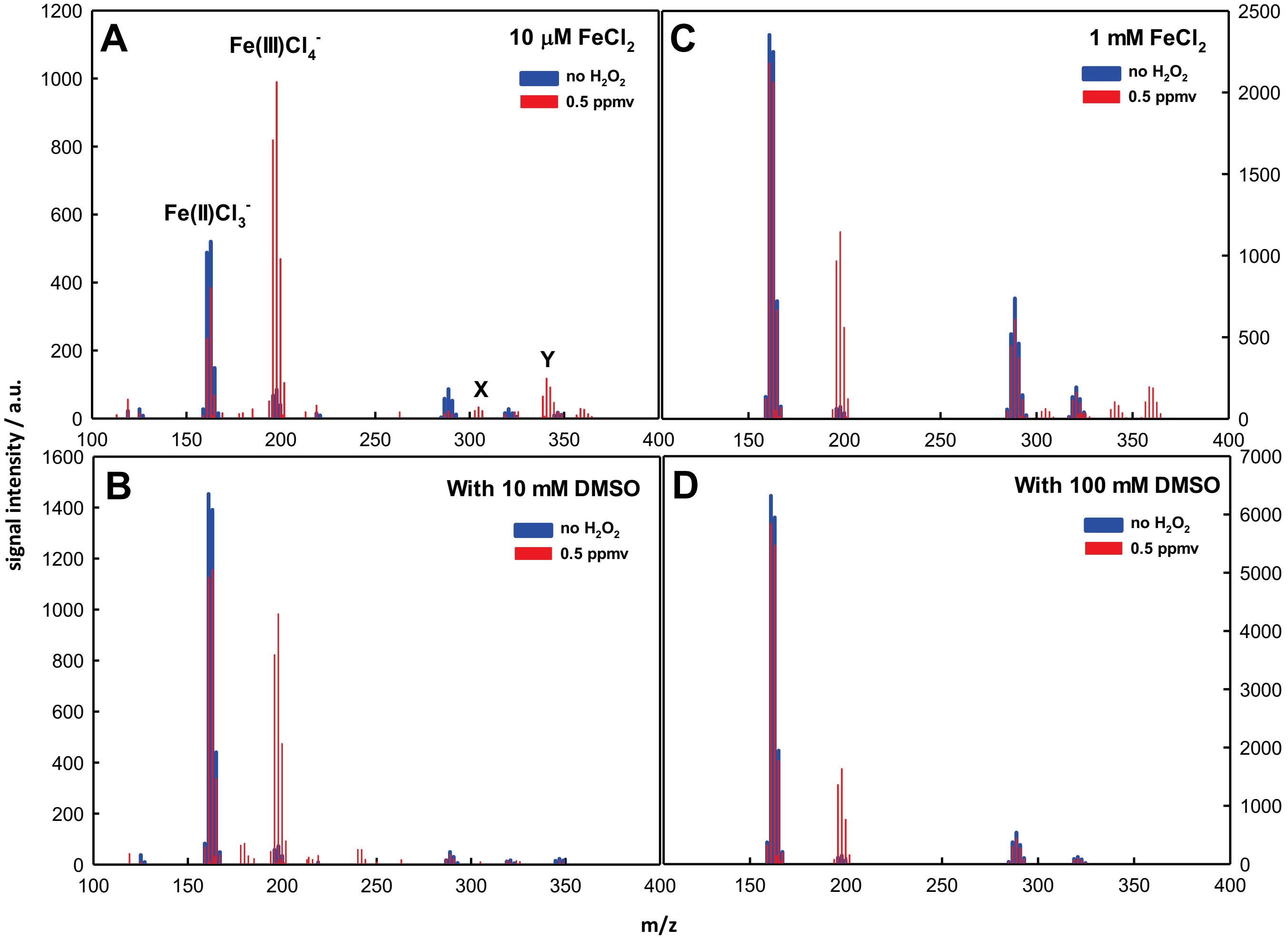

Fig. S4. Negative ion electrospray mass spectra of aqueous microjets containing 10 μM $FeCl_2$ in the absence (*A*)/presence (*B*) of 10 mM DMSO and 1 mM $FeCl_2$ in the absence (*C*)/presence (*D*) of 100 mM DMSO exposed by H_2O_2(g) for ∼10–50 μs. X and Y correspond to $O{=}Fe^{IV}{\cdot}Cl{\cdot}Fe^{II}Cl_4^-$ and $O{=}Fe^{IV}{\cdot}Cl{\cdot}Fe^{III}Cl_5^-$, respectively.

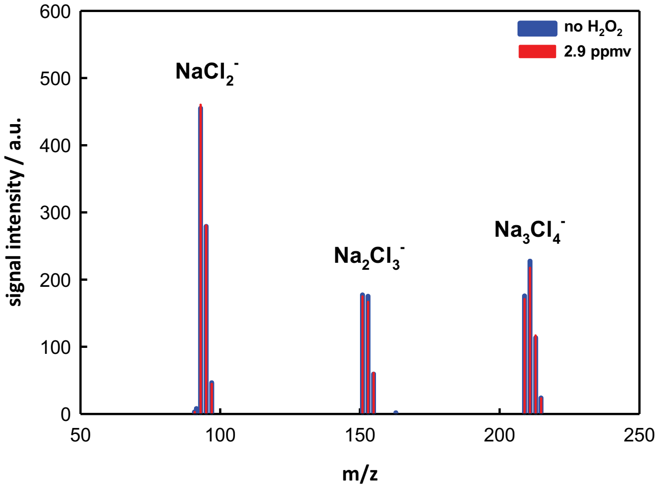

Fig. S5. Negative ion electrospray mass spectra of aqueous microjets containing 1 mM NaCl in the absence/presence of H_2O_2(g). Note that Cl^- does not react with H_2O_2 under the present condition.